Optimizing rheological behavior of glass-based sealant inks for robocasting deposition: A design of experiment approach

Materials & Design 251 (2025) 113678

Contents lists available at ScienceDirect

Materials & Design

journal homepage: www.elsevier.com/locate/matdes

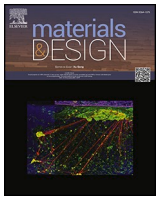

Optimizing rheological behavior of glass-based sealant inks for robocasting deposition: A design of experiment approach

A. Baggio [a,*], D. Dalmazzo [b], F. D'Isanto [a], E. Santagata [c], D. Basso [d], D. Gaia [d], M. Salvo [a], F. Smeacetto [a]

[a] Politecnico di Torino, Department of Applied Science and Technology – DISAT, Corso Duca degli Abruzzi 24, 10129 Torino, Italy
[b] Politecnico di Torino, Department of Environmental, Land and Infrastructure Engineering – DIATI, Corso Duca degli Abruzzi 24, 10129 Torino, Italy
[c] Qatar University, Department of Civil and Environmental Engineering, P.O. Box 2713, Doha, Qatar
[d] FZSoNick S.A., Via Laveggio 15, 6855 Stabio, Switzerland

ARTICLE INFO

Keywords:
Rheology
Glass-based sealant
Robocasting
Design of Experiment
Fractional Factorial Design
Joining

ABSTRACT

Robocasting is a commonly used method for depositing ceramic and glass inks, especially for glass-based sealants. Developing an ink recipe that optimizes an existing process can be a complex and time-consuming task. This study utilized a statistical approach based on the Design of Experiment theories to fine-tune the rheological properties of a water-based glass-based suspension with a limited number of experiments.

The key components of the sealant were characterized with a scanning electron microscope, and a fractional factorial design $2^{(5-1)}$ was implemented to investigate the influence of each component on the rheological characteristics of the ink within a predefined domain of variation. The information obtained and the resulting models were useful in designing a new formulation that closely mimics the rheology of a state-of-the-art ink formulation.

This analytical approach not only facilitated the development of a new sealant ink but also enabled its seamless integration into an existing industrial robocasting deposition process without requiring additional adjustments. The study contributes to a better understanding of the influence of each ink component on the rheological behavior and to the design of a new formulation with rheological characteristics very close to those of a reference paste.

1. Introduction

Glass-based materials have been extensively studied since the 1990 s as versatile sealants for joining advanced ceramics, ceramic matrix composites, and ceramic-to-metal components for high-temperature and harsh environment applications [1–6]. One of the most appealing characteristics of glass is the straightforward manner in which its properties can be manipulated by altering its chemical composition. Thus, it is possible to tailor important properties such as the Coefficient of Thermal Expansion (CTE), the glass-transition temperature (Tg), and chemical stability [7,8] by properly tuning the amount of oxides that form the glass. These properties are selected based on the specific application for which the sealant has been designed. The energy sector is one of the fields of application for this class of joining materials. For example, glass and glass–ceramic sealants are used to assemble energy conversion and storage devices, such as Solid Oxide Cells and batteries. Molten Sodium Batteries, including Na-NiCl, Na-S, and Na-ZnCl, are state-of-the-art technologies for stationary storage systems due to their high energy density, long lifetime, and improved safety compared to other alternatives [9–11]. These types of batteries require high operating temperatures ranging from 270-350 °C and work in corrosive environments, mainly due to the presence of sodium – both liquid and vapor – and molten salts [12–14]. For this application, the sealant should be thermo-mechanical compatible with the β''-alumina electrolyte, ensuring proper tightness between the cathode, anode, and external environment, and establishing strong bonds between the alumina components [15]. Several examples of the successful use of glass and glass–ceramic sealants, including the Na-ZnCl solid electrolyte battery have been reported in the literature [15–20]. As part of the SOLSTICE EU project (www.solstice-battery.eu), a new joining material has been developed to lower by approximately 100 °C the sealing temperature currently used by FZSoNick SA company to assemble the ZEBRA®

* Corresponding author.
E-mail address: andrea.baggio@polito.it (A. Baggio).

https://doi.org/10.1016/j.matdes.2025.113678
Received 13 August 2024; Received in revised form 28 January 2025; Accepted 28 January 2025
Available online 29 January 2025

battery, reducing the energy consumption. The newly glass-based sealing system must be deposited on one of the substrates using an automatic industrial process that has already been optimized for the water-based ink composed of the glass system currently used by the company in its manufacturing process.

The robocasting technique was introduced in 1996 [21] and nowadays has become one of the most versatile additive manufacturing technologies for in-situ deposition of glass and glass–ceramic powders [22–25]. It has also been explored as a reliable solution for the controlled deposition of sealants [26,27]. To improve control over paste printability and the shape fidelity of extruded material during ink direct deposition, it is essential to precisely adjust the rheological behavior of powder suspensions [28,29]. Indeed, the inks must possess suitable rheological properties, displaying a shear-thinning behavior during the printing process and consistency after its deposition. However, robocasting inks are complex systems composed of various components, including the solid load (the sealant itself), the solvent, plasticizers, and surfactants [30]. The equilibrium of the system depends on a delicate balance of its components, each exerting a distinct influence on the ink's flow behavior.

A comprehensive study of the effect of each component can be challenging and time-consuming, particularly with the common approach of varying one variable at a time. In contrast, the Design of Experiment (DoE) is a multivariate approach that can be highly beneficial in studying complex systems. This statistical approach, first introduced by Ronald Fisher in 1935 [31], has been successfully adopted in many different fields, including pharmaceutics [32–34], wire bonding [35,36], water treatments [37,38], and many others [39–42]. This approach analyzes how a certain system is modified by changes in the value of variables or factors, by measuring responses. The DoE allows for the creation of mathematical models that can accurately predict the value of a response at any point within the experimental domain [43–45]. This statistical approach has been used to optimize additive manufacturing processes [40,46,47], such as in the case of A. Renteria et al. who improved the performance of a piezoelectric device by controlling four different printing parameters [48]. Moreover, I. Buj-Corral et al. successfully used DoE to correlate variations in printing parameters with the roughness and dimensional errors of printed ceramic prostheses [49].

However, for industrial-scale applications, modifying the direct deposition process by altering machine-specific printing parameters is not always feasible, as such adjustments can disrupt the efficiency of the production line. Consequently, the ability to tailor the rheological behavior of inks based on their recipe to accommodate a standardized printing process, rather than adapting the method to the ink, presents a compelling and practical approach. To the best of the authors' knowledge, existing studies on the optimization of printing processes through tuning the inks' recipes usually considered the effect of one costituent at a time, lacking a holistic overview af the whole system [24,50–52].

Thus, this study aimed to develop a replicable methodology for investigating the influence of ink composition on its rheological properties. This was achieved using DoE combined with analysis of variance (ANOVA) to optimize ink formulations capable of consistent performance under fixed printing parameters. Furthermore, the study introduced novel indexes to support the standardization of a common definition of printability in robocasting deposition, addressing a critical challenge identified by the scientific community [24,29]. These indexes are intended to serve as a foundation for advancing both practical applications and theoretical understanding in this domain.

2. Materials & Methods

The reference ink (labeled as Ref), is a water-based suspension composed of a solid load, a solvent, and several additives acting as rheology modifiers. The solid load consists of a mixture of commercial glass and alumina powder (> 95 % pure), while the solvent used has been deionized water. The rheology modifiers used for this ink are bentonite (sodium form, A15795) [53,54], microfine NaCl (Custom Powders Ltd, Gateway, United Kindom) [55–57], and fumed silica (Merck KGaA, Darmstadt, Germany) [58,59]. To guarantee the best homogeneity possible in the preparation of the inks, all the constituents were used from a singular batch. However, based on the robust experience of FZSoNick, the variability introduced by employing different batches does not result in substantial alterations to the inks' rheology.

In previous work, F. D'Isanto et al. [60] developed a new sealant based on the commercial silica-based G018-402 glass specifically developed by SCHOTT AG (Landshut, Germany) for the hermetic sealing and joining of ceramics and/or metals in highly corrosive environments, such as molten sodium batteries. The chemical composition of this glass and the Ref one has been reported in Table 1. The G018-402 glass system has been successfully modified by adding alumina powder (> 95 % pure) and Li_2CO_3 powder (Merck KGaA, Darmstadt, Germany) to improve the wettability on alumina substrates at the sealing temperature. This new sealant was used to substitute the solid load of the Ref ink, obtaining a new formulation of the ink labeled GL. Both the Ref and the GL inks have been prepared by weighing the correct amount of distilled water. The microfine NaCl was first dissolved inside, followed by the addition of fumed silica and bentonite. The obtained compound was homogenized on a roller mixer for 30 min at a speed of 60 rpm. The solid load mixture has also been prepared and mixed following the same procedure just presented. Finally, the solid load was added to the other components of the ink and the final suspension was mixed for 18 h on the roller mixer.

For the first screening, the sedimentation time of the Ref and GL inks has been observed, resulting in a very poor stability of the second formulation. For this reason, the powders of Ref glass and G018-402 glass, together with the Li_2CO_3, have been observed and compared in morphology by a Field-Emission Scanning Electron Microscope (FESEM) (MIRA3, TESCAN). The grain size distribution has been also measured by considering the dimension of at least 200 particles, calculated by using ImageJ software.

To increase the suspension stability of GL ink, Targon 899 was introduced in the formulation as a dispersant [61,62], leading to the recipe named GLT. All the inks' recipes are presented in Table 2. Since the composition of the Ref ink is commercially sensitive information, ranges rather than exact values are provided.

2.1. Design of Experiment

Starting from the GLT formulation previously defined, the DoE approach has been applied to analyze the experimental space around this formulation. By considering the solid load as a unique component, the GLT ink is then constituted by the following six ingredients: solid load, water, bentonite, fumed silica, NaCl, and Targon.

In the context of studying the composition of a mixture in the DoE, it is important to note that each constituent cannot be regarded as a wholly independent variable. This is due to the requirement that the total sum must equal 100 % [43]. In such instances, employing of a Mixture Design becomes essential [63–65]. However, R. Leardi et al. [43] previously reported that in cases involving more than four constituents, applying of a Mixture Design can be challenging, necessitating the division of the system into smaller Mixture Designs comprising no more than four

Table 1
Chemical composition of both Ref and G018-402 glasses.

	Ref glass	G018-402
SiO_2	40–50 wt%	40–50 wt%
B_2O_3	20–30 wt%	>25–30 wt%
Al_2O_3	9–12 wt%	17–25 wt%
Na_2O	3–5 wt%	5–15 wt%
MO (MgO + CaO + SrO + BaO)	10–18 wt%	<2 wt%
Others (K_2O + ZnO + TiO_2 + SnO_2)	< 1.5 wt%	0–5 wt%

Table 2
Inks recipe of the Ref paste, the GL, which introduces G018-402 glass and Li_2CO_3 in the solid load, and GLT, where Targon has been added to the GL formulation to increase the suspension stability.

Role	Substance	Ref	GL	GLT
solvent	water	**34–38 wt%**	**34–38 wt%**	**35.87 wt %**
rheology modifiers	Bentonite	**0.6–1.4 wt %**	**0.6–1.4 wt %**	**1.29 wt%**
	fumed silica	**0.1–0.2 wt %**	**0.1–0.2 wt %**	**0.12 wt%**
	NaCl	**<0.1 wt%**	**<0.1 wt%**	**0.03 wt%**
	Targon	–	–	**1.23 wt%**
solid load		**60–65 wt%**	**60–65 wt%**	**61.46 wt %**
	Ref glass	74–77 wt%	–	–
	G018-402	–	74 wt%	74 wt%
	Li_2CO_3	–	2 wt%	2 wt%
	alumina	23–26 wt%	24 wt%	24 wt%

variables. However, the system studied in the present work – and inks for robocasting in general – exhibited a distinctive characteristic: except or solvent (water) and solid load, the remaining components possessed a negligible concentration, falling below 5 % in total. Consequently, it was feasible to consider bentonite, fumed silica, NaCl, Targon and solid load as independent variables, with water being regarded as dependent on the others. This assumption facilitated the utilization of a fractional factorial design 2^{5-1} [66], a methodology that has been identified as more convenient for the study of the interactions between each couple of variables. This kind of model requires the definition of two different levels for each variable (i.e. the minimum and the maximum values the variable assumes during the experiments) coded as –1 and 1. The level corresponding to the intermediate value is coded as 0. As mentioned later, the recipe with all variables at level 0 will be used to measure the experimental error associated with the measurements and to validate the models that have been postulated. The value of the variables at all levels is given in Table 3.

The resulting equation of the model is reported as follows:

$$
\begin{aligned}
Y = {} & b_0 + \\
& + b_1(X_1 + X_2X_3X_4X_5) + b_2(X_2 + X_1X_3X_4X_5) + b_3(X_3 + X_1X_2X_4X_5) + b_4(X_4 + X_1X_2X_3X_5) + b_5(X_5 + X_1X_2X_3X_4) + \\
& + b_{12}(X_1X_2 + X_3X_4X_5) + b_{13}(X_1X_3 + X_2X_4X_5) + b_{14}(X_1X_4 + X_2X_3X_5) + b_{15}(X_1X_5 + X_2X_3X_4) + \\
& + b_{23}(X_2X_3 + X_1X_4X_5) + b_{24}(X_2X_4 + X_1X_3X_5) + b_{25}(X_2X_5 + X_1X_3X_4) + \\
& + b_{34}(X_3X_4 + X_1X_2X_5) + b_{35}(X_3X_5 + X_1X_2X_4) + \\
& + b_{45}(X_4X_5 + X_1X_2X_3)
\end{aligned}
\tag{1}
$$

Table 3
List of the variables taken into account in the fractional factorial design, their corresponding names, and coded values.

Fractional factorial design $2^{(5-1)}$ Component	Variable name	Coded values −1	0	1
Bentonite	X_1	1 wt%	1.3 wt%	1.6 wt%
Fumed silica	X_2	0.09 wt%	0.12 wt%	0.15 wt%
NaCl	X_3	0.01 wt%	0.03 wt%	0.05 wt%
Targon	X_4	0 wt%	1.2 wt%	2.4 wt%
solid load	X_5	58.5 wt%	61.5 wt%	64.5 wt%

Table 4
Experimental matrix for the fractional factorial design. List of the experiments carried out with the corresponding coded values for each variable of the system.

Experimental matrix Sample	X_1	X_2	X_3	X_4	X_5
GLT1	−1	−1	−1	−1	1
GLT2	1	−1	−1	−1	−1
GLT3	−1	1	−1	−1	−1
GLT4	1	1	−1	−1	1
GLT5	−1	−1	1	−1	−1
GLT6	1	−1	1	−1	1
GLT7	−1	1	1	−1	1
GLT8	1	1	1	−1	−1
GLT9	−1	−1	−1	1	−1
GLT10	1	−1	−1	1	1
GLT11	−1	1	−1	1	1
GLT12	1	1	−1	1	−1
GLT13	−1	−1	1	1	1
GLT14	1	−1	1	1	−1
GLT15	−1	1	1	1	−1
GLT16	1	1	1	1	1
GLT17	0	0	0	0	0
GLT18	0	0	0	0	0
GLT19	0	0	0	0	0
GLT20	0	0	0	0	0

Thus, by using the ANOVA it is possible to evaluate the effect of the single variable (X_n) and its mutual interaction with another one (X_nX_m), although the responses could be confused with the interactions of a higher grade (triple, quadruple, etc.). This means that the same coefficient (b_1 for instance) can describe the effect of two different phenomena at the same time (the change in X_1 and the interaction between all other factors). Perhaps, it has been demonstrated that interactions of a grade higher than 2 are commonly very rare, so it is possible to consider them negligible [66].

Since the postulated model has 16 degrees of freedom, the same number of experiments is necessary to define them. Thus, one experiment in each edge points of the five-dimension hyperspace described in Table 3 was performed, allowing the calculation of each coefficient b_n in Equation (1). In addition, 4 more experiments were conducted at the central point of the model, with all variables at level 0, to estimate the experimental error and to validate the model prediction accuracy. Consequently, the experimental matrix composed of a total of 20 experiments has been defined as reported in Table 4. For instance, the sample GLT3 was made by adding to the water 1 wt% of bentonite (X_1 = -1), 0.15 wt% of fumed silica (X_2 = 1), 0.01 wt% of NaCl (X_3 = -1), 0 wt % of Targon (X_4 = -1), and 58.5 wt% of solid load (X_5 = -1). All the computations and the plots related to the DoE were generated by the software CAT 4.3.

2.2. Rheological characterization

A rotational rheometer (Anton Paar Physica MCR 301) equipped with coaxial cylinders (CC17/T200/SS) was used to characterize all the different compositions of paste by means of a Flow Sweep Test (FST) and a 5-Interval Thixotropy Test (5ITT). All the measurements were performed at a temperature of about (25 ± 1)°C, which was detected directly by the instrument. In the FST the shear rate was varied from 0.01 s^{-1} to 1000 s^{-1} and back to 0.01 s^{-1} and 51 measurements were collected every 5 s. Then, the obtained characteristic curves were used to evaluate the Newtonian or non-Newtonian behavior of the powder suspensions. On the other hand, the 5ITT aimed to investigate the rheological response of the inks under conditions that mimic the printing process. In particular, the 5ITT was set as follows:

- Step 1: $\dot{\gamma} = 0.01\ s^{-1}$; interval time = 30 sec; 6 pts
- Step 2: $\dot{\gamma} = 60\ s^{-1}$; interval time = 30 sec; 6 pts
- Step 3: $\dot{\gamma} = 0.01\ s^{-1}$; interval time = 120 sec; 24 pts
- Step 4: $\dot{\gamma} = 60\ s^{-1}$; interval time = 30 sec; 6 pts
- Step 5: $\dot{\gamma} = 0.01\ s^{-1}$; interval time = 120 sec; 24 pts

The shear rate of 0.01 s^{-1} was meant to reproduce the paste at rest (i.e. inside the syringe and after the deposition), while 60 s^{-1} is the shear rate associated with the maximum stressed condition at which the paste is subjected at the exit to the nozzle. This value was estimated by [67]:

$$\dot{\gamma} = \frac{4\dot{Q}}{\pi r^3} \tag{2}$$

where $\dot{\gamma}$ is the maximum shear rate in a cylindric nozzle of diameter r equal to 1 mm and the volumetric flow rate $\dot{Q}$ of 0.04–0.05 ml/s. The resulting shear rate is in the range of 50.9–63.7 s^{-1}.

From the 5ITT results, 14 different parameters have been defined, in order to quantitatively describe the inks response. Table 5 collects all the parameters, with their definition and meaning. The coefficients of variation (Y2, Y2′, Y6, and Y6′) were calculated according to the following equation:

$$e = \sqrt{\frac{\sum_{i=1}^{n} (\eta_i - \eta_n)^2}{n}} \cdot \frac{1}{\eta_n} \tag{3}$$

where e is the generic coefficient of variation, η is the viscosity measured by the instrument at one specific point i, and n is the number of points measured in the step under consideration (equal to 6 for Y2 and Y2′, and 24 for Y6 and Y6′).

Table 5
A list of all the responses analyzed with the DoE correlated with the given definition and a brief explanation of the purpose of the specific response.

Parameter	Definition	Meaning
Y1	stabilized viscosity at step 2: first point which differs from the viscosity of the last point of the step by less than 2 %	viscosity of the paste at the nozzle exit
Y1′	stabilized viscosity at step 4: first point which differs from the viscosity of the last point of the step by less than 2 %	viscosity of the paste at the nozzle exit
Y2	coefficient of variation, referred to as the stabilized value, of the viscosity points measured in step 2	measuring how much stable is the viscosity of the ink during this step
Y2′	coefficient of variation, referred to as the stabilized value, of the viscosity points measured in step 4	measuring how much stable is the viscosity of the ink during this step
Y3	ratio between Y1 and Y1′	measuring the reproducibility of the rheological behavior during two consecutive prints
Y4	ratio between Y2 and Y2′	measuring the reproducibility of the rheological behavior during two consecutive prints
Y5	stabilized viscosity at step 3: first point which differs from the viscosity of the last point of the step by less than 2 %	viscosity of the paste after deposition
Y5′	stabilized viscosity at step 5: first point which differs from the viscosity of the last point of the step by less than 2 %	viscosity of the paste after deposition
Y6	coefficient of variation, referred to as the stabilized value, of the viscosity points measured in step 3	measuring how much stable is the viscosity of the ink during this step
Y6′	coefficient of variation, referred to as the stabilized value, of the viscosity points measured in step 5	measuring how much stable is the viscosity of the ink during this step
Y7	ratio between Y5 and Y5′	measuring the reproducibility of the rheological behavior after two consecutive prints
Y8	ratio between Y6 and Y6′	measuring the reproducibility of the rheological behavior after two consecutive prints
Y9	the stabilization time of step 3	time passed before viscosity reaches the stabilized value from the beginning of step 3
Y9′	the stabilization time of step 5	time passed before viscosity reaches the stabilized value from the beginning of step 5

3. Results and discussion

As previously mentioned, the present study aims to replace the commercial glass of the existing Ref ink – which is listed in Table 2 – with a mixture of the G018-402 silica-based glass and Li_2CO_3, guaranteeing similar sealing performances while decreasing the temperature of the joining process.

In the development of inks for robocasting, it is well known that the rheological properties of a suspension are greatly influenced by the composition and the morphology of its constituent particles.

For this reason, SEM imaging has been used to investigate the size and shape of the powder grains. Fig. 1 shows micrographs and the corresponding grain size distribution of the Ref glass, G018-402, and Li_2CO_3 powders. It is evident that no significant difference in shape or size is observable between the powders of the two glasses, while the carbonate presented a completely different grain morphology, with a D50 and a mean grain size about three times higher than the one of both the glass powders. On the other hand, focusing on the composition of the two glasses reported in Table 1, one can notice the higher amount of alumina in the G018-402 silica-based system (>17 wt%), compensated by a lower presence of alkaline-earth oxides (under 2 wt%, compared with 10–18 wt% of the Ref glass).

Indeed, once the ink was prepared using the new glass, GL ink in Table 2, a significant modification in the behavior of the paste was observed: the suspension was not as stable as the Ref ink, demonstrating a visible separation after 30 min of resting time, as shown in Fig. 2. The modification in the composition of the glass powder, as well as the presence of an additional component with a different granulometry – i.e. Li_2CO_3 – is sufficient to modify the equilibrium within the suspension. For this reason, it has been necessary to introduce into the ink a dispersant, Targon, which improved the stabilization leading to the GLT formulation.

As previously presented in the DoE section, based on the GLT formulation, a fractional factorial design 2^{5-1} was defined and an experimental matrix of 20 samples was obtained (Table 4). Thus, all the different ink formulations were prepared and rheologically characterized by FST and 5ITT tests in a randomized order. The FST has revealed a

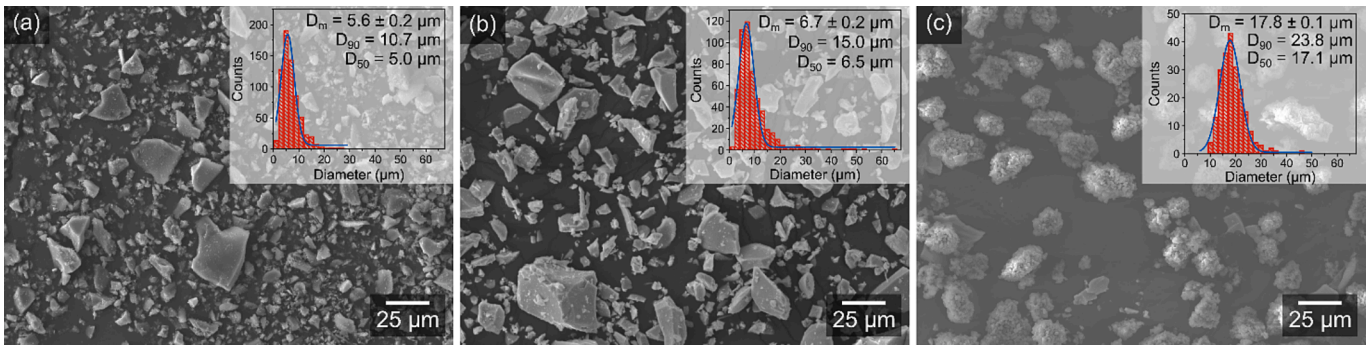

Fig. 1. SEM picture of the (a) Ref glass powder, (b) G018-402 glass powder, and (c) Li_2CO_3 powder, and the corresponding particle size distribution graphs reporting the mode of diameters (D_m), D_{90}, and D_{50}.

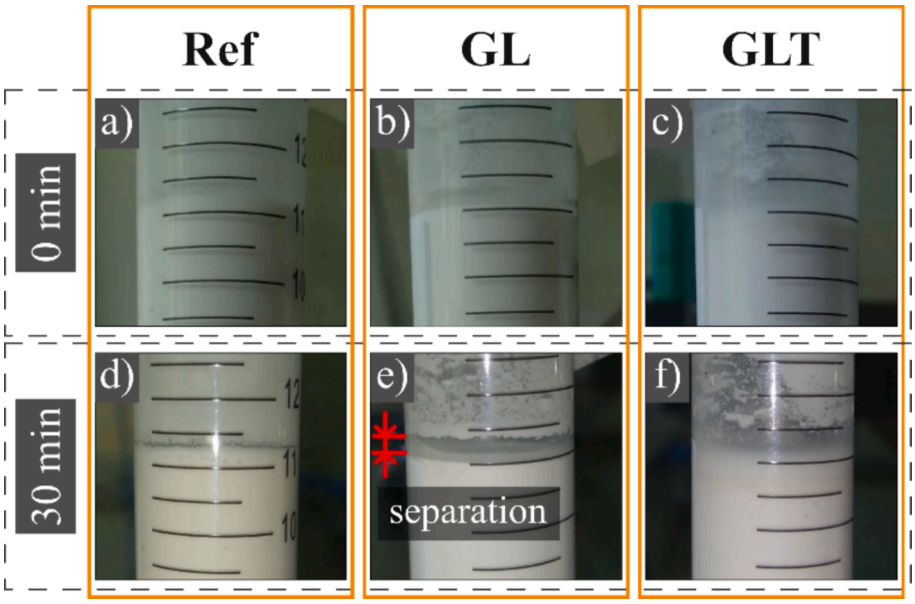

Fig. 2. Pictures of a centrifuge tube filled with Ref, GL, and GLT before (a, b, and c, respectively) and after 30 min of resting time (d, e, and f, respectively). Ref and GLT suspensions looked stable during the detection time, while GL showed a slice phase separation (e).

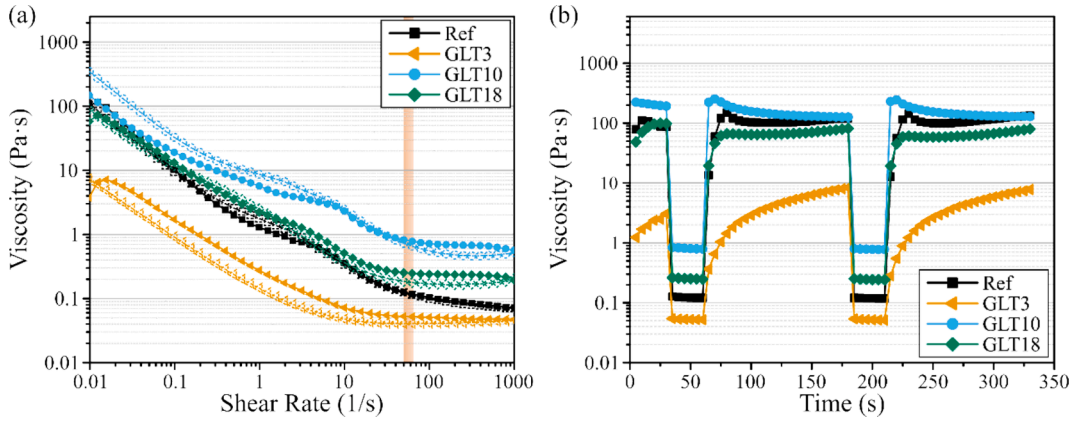

Fig. 3. (a) Curves obtained by the Flow Sweep Test conducted on the paste Ref, GLT3, GLT10, and GLT18. The dashed curve represents the viscosity during the step of decrease of shear rate from 1000 to 0.01 s^{-1}. (b) 5-Interval Thixotropy curves corresponding to the same samples.

shear thinning behavior, characterized by an exponential decrease in viscosity as the shear rate increases, of all the tested formulations, which constitutes a key factor in robocasting deposition [68]. Some of the most representative curves from this test are reported in Fig. 3a, in which the interval of the shear rate expected at the nozzle outlet is highlighted by a colored bar. In particular, GLT3 and GLT10 – i.e., the experimental points [-1; 1; −1; −1; −1] and [1; −1; −1; 1; 1], respectively – represented the formulations that described the two extreme responses, considering the FST test, while GLT18 is the one that best reproduces the reference characteristic curve. By changing the composition of the ink,

the viscosity value at the shear rate at the nozzle exit varies in a wide range, i.e. 0.04–0.9 Pa•s. As expected, it was observed that the highest viscosity values were obtained for high concentrations of bentonite, Targon, and solid load (e.g. GTL10). Similar considerations on the variation in viscosity as a function of composition can be made by analyzing the 5ITT results shown in Fig. 3b. Looking at how the viscosity varies when going from high to very low strain rates, a marked thixotropy is observed for the GL3 paste.

To investigate further the existing correlations between the inks' formulation and their rheological behavior, the DoE was used. Based on the 5ITT curves, the 14 indexes listed in Table 5 were used as Y responses in a $2^{(5-1)}$ fractional factorial design and the corresponding models have been calculated with the CAT software. Moreover, the four replications at the central point (GLT17-GLT20) were used to estimate the standard deviation and thus experimental error associated with these measurements. The hypothesis of homoscedasticity within the analyzed experimental domain was useful to easily validate the models by comparing the real value measured in point (0,0,0,0,0) – the four replications – and the one predicted by the model, both net to the uncertainty related to both values as indicated by B. Benedetti et al. [44].

From this analysis, the models associated with the coefficient of variation of the rheological characteristics (i.e. Y2, Y2′, Y6, and Y6′) were not validated and then discarded. This result demonstrated the impossibility of describing the effect of the selected variables using the linear model described in Equation (1) in the limits of the experimental domain defined in Table 3. Thus, it may be necessary to introduce quadratic terms or, alternatively, modify the definition of the coefficient of variation. On the other hand, the remaining models were all validated and used to analyze the effect of individual components (such as bentonite, fumed silica, NaCl, Targon, and solid load) and their mutual interactions on the rheological response during the different phases of the ink printing process.

By evaluating the coefficients (b_n) associated with each variable (X_i) and their mutual interactions (X_iX_j), it is possible to estimate the influence that a variation in the dosage of a specific component has on the final response Y. Examining Equation (1), it becomes clear that it is the values of the coefficients associated with the variables (or their mutual interactions) that determine the response value predicted by the model. Therefore, the greater the value of the coefficient associated with a certain variable, the greater its impact on the predicted response. Furthermore, when a coefficient b_n assumes positive values, an increment in the amount of the corresponding component (X_i) leads to an increment of the value of the generic response Y. On the contrary, an increment of a component's concentration can be associated with a decrease in the value of the response Y when the corresponding coefficient b_n is lower than zero.

As shown in Fig. 4a and Fig. 4b, the viscosity of the paste at the nozzle exit (Y1, Y1′) is primarily affected by the solid load content (variable X_5) – characterized by the higher value of the coefficient b_5 and a p-value lower than 0.001, followed by bentonite (X_1) and Targon (X_4) with $p < 0.01$, and NaCl (X_3) with $p < 0.05$. Among the considered interactions, only the ones involving solid load are relevant (X_4X_5 with $p < 0.01$, X_1X_5, and X_3X_5 with $p < 0.05$).

On the other hand, looking at Fig. 4c and Fig. 4d, the viscosity of the

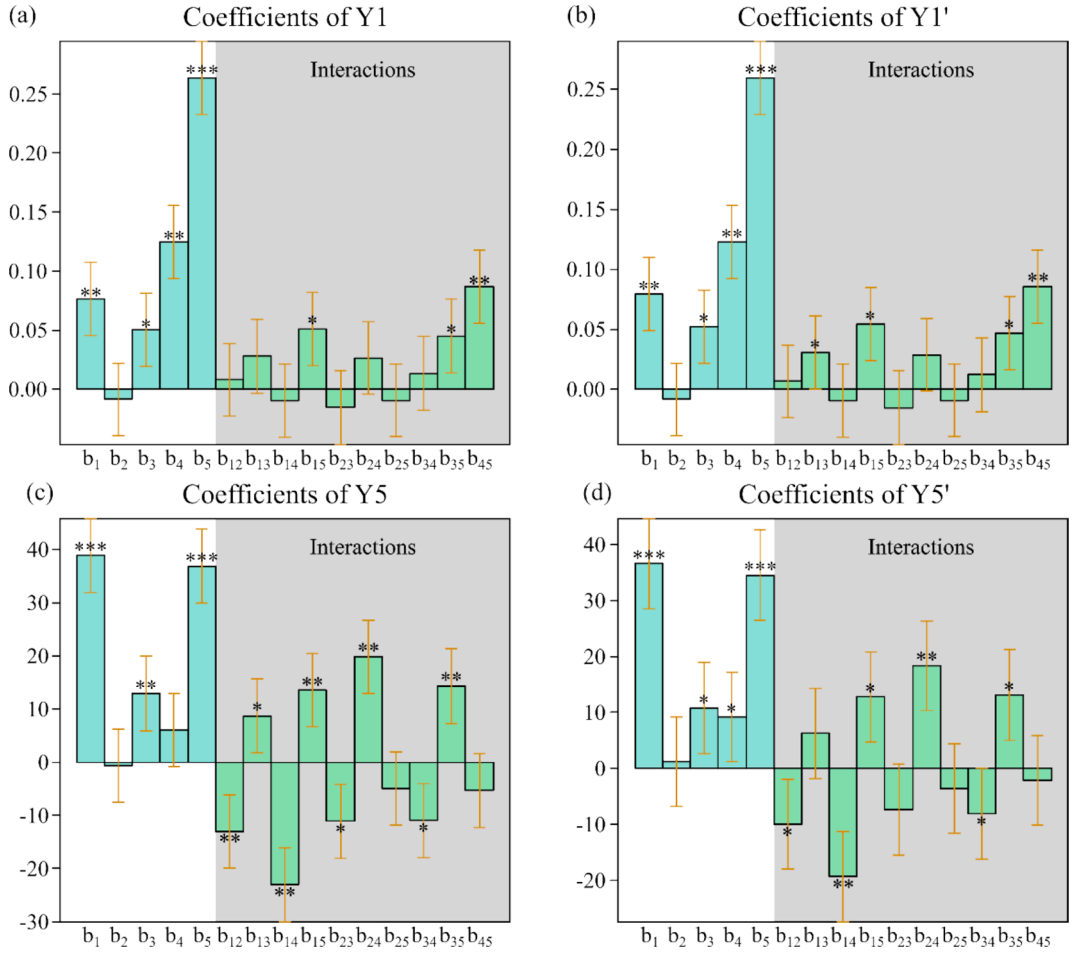

Fig. 4. Plots of the coefficients of the models corresponding to (a) Y1, (b) Y1′, (c) Y5, and (d) Y5′. Each bar corresponds to the value of the coefficient referred to a variable or a specific interaction. The number of asterisks indicates the p-value for each coefficient: * indicates $p < 0.05$, ** indicates $p < 0.01$, and *** indicates $p < 0.001$.

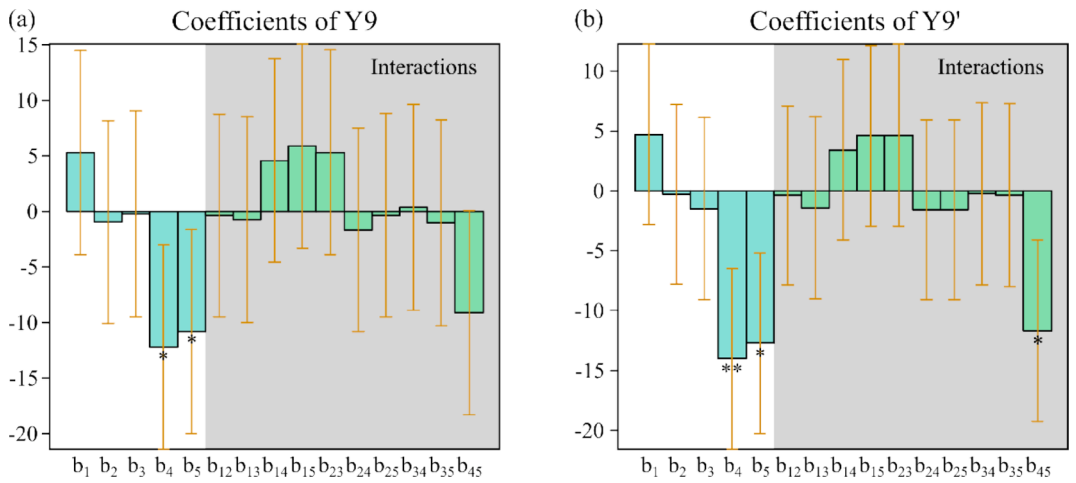

Fig. 5. Plots of the coefficients of the models corresponding to (a) Y9 and (b) Y9′. Each bar corresponds to the value of the coefficient referred to a variable or a specific interaction. The number of asterisks indicates the p-value for each coefficient: * indicates $p < 0.05$, ** indicates $p < 0.01$, and *** indicates $p < 0.001$.

paste after deposition (Y5 and Y5′) is mainly affected by bentonite (X_1) and solid load (X_5) with $p < 0.001$. At this stage, mutual interactions, particularly those related to bentonite, become more relevant. The broader influence of bentonite on the ink viscosity after deposition can be justified by the randomized orientation of the clay platelets when at rest. Indeed, at the nozzle exit, the platelets tend to align, creating preferred planes of shifting. For this reason, at high shear rates, the bentonite dosage becomes less relevant. These results are in agreement with what was already observed by Y. Liu et al. on the influence of bentonite concentration on the viscosity of a water suspension [69]. Moreover, the presence of Targon, acting as a dispersant, increases the ink's viscosity, with its effect more evident at high shear rates.

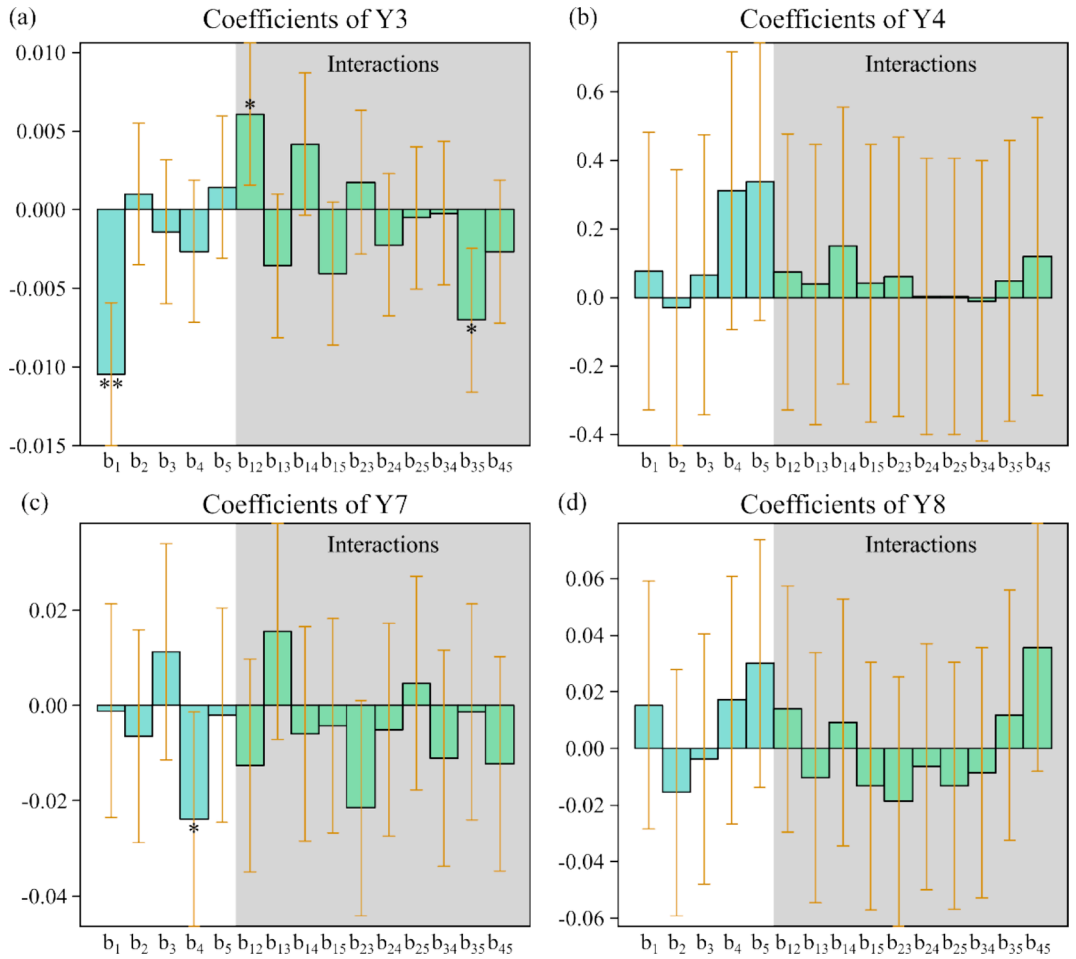

Fig. 6. Plots of the coefficients of the models corresponding to (a) Y3, (b) Y4, (c) Y7, and (d) Y8. Each bar corresponds to the value of the coefficient referred to a variable or a specific interaction. The number of asterisks indicates the p-value for each coefficient: * indicates $p < 0.05$, ** indicates $p < 0.01$, and *** indicates $p < 0.001$.

The responses Y9 and Y9′, representing the time passed before viscosity reaches a constant value in steps 3 and 5 respectively, were used to monitor the speed at which the ink recovers its original stabilized internal structure after deposition. These parameters are important because they return information on the ability of the ink to maintain the given shape after printing. Fig. 5 reports the coefficients calculated by the model and it shows that a higher concentration of solid load and Targon leads to a decrease in stabilization time. In particular, for Y9 the influence of these two components on the stabilization time is lower (equal to −12.2 and −10.8 for b_4 and b_5, respectively, with a $p < 0.05$) with respect to the stabilization time after the second deposition Y9′ (b_4 and b_5 equal to −14.0 and −12.7 with a $p < 0.01$ and $p < 0.05$, respectively). Moreover, Fig. 5b shows that an increase in the concentration of Targon and the solid load conducts in a decrease in the stabilization time at the second consecutive printing process, not only for the effect of the two components separately, but also for their mutual interaction, with a $p < 0.05$.

As regards the response measuring the viscosity stability during two consecutive printing processes (i.e. Y3), as shown in Fig. 6a, this is mainly influenced by bentonite (b_1) and its interactions with fumed silica (b_{12}), with $p < 0.01$ and $p < 0.05$ respectively. The interaction between NaCl and solid load (b_{35}) also appears to influence Y3, with a $p < 0.05$.

The other coefficients that look at the stability of the rheological properties of the ink in two consecutive printing processes (i.e. Y4, Y7, and Y8) are negligibly influenced by the concentration of the components in the range of variation considered. As shown in Fig. 6, only Targon is expected to influence the stability of the viscosity after deposition (i.e., Y7), with a low p-value (equal to 0.04).

The models presented above were also used to explore the experimental space defined by the variation range of each variable (Table 3) and find the ink composition whose responses Y correspond to the ones of the Ref paste.

From the previous analysis, it has been demonstrated that X_2 and X_3 do not have a significant influence on the majority of the predicted responses, while bentonite (X_1), Targon (X_4), and solid load (X_5) demonstrated an important effect. For this reason, the optimized recipe of the ink was selected from 342 potential candidates, which represent all the possible combinations obtained by varying the values of X_1, X_4, and X_5 among seven equally spaced values (corresponding to the coded values −1.00, −0.66, −0.33, 0.00, 0.33, 0.66, 1.00), while X_2 and X_3 were considered constant and set to the coded value 0 (corresponding to a concentration of 0.12 wt% and 0.03 wt%, respectively). All the different recipes were identified by assigning them with a number from 1 to 342 (all the recipes were reported in the Supplementary S1). Subsequently, the previously presented models were used to calculate the predicted value for each Y response associated with all the recipes considered. The predicted responses, plotted in Fig. 7, were compared to the ones measured on the Ref ink, represented by the green-colored areas on the charts.

From Fig. 7a, Fig. 7i, and Fig. 7j, it is evident that two main macro-families can be observed. One group of recipes with a high concentration of Targon and solid load (respectively X_4 and X_5 coded > 0) have stabilization time values (Y9 and Y9′) comparable to the Ref ink. On the other hand, several ink formulations have a viscosity at 60 s^{-1} (Y1 and Y1′) similar to the Ref, but with higher stabilization times. These inks are constituted by a lower amount of Targon and solid load. In fact, from the analysis of the coefficients reported in Fig. 4a, Fig. 4b, and Fig. 5, it was observed that X_4 and X_5 have opposite effects on viscosity at 60 s^{-1} and stabilization time. Specifically, as the value of X_4 and X_5 increases, an increase is observed on Y1 and Y1′, but a consequent decrease on Y9 and Y9′ is faced.

Hence, some criteria of selection have to be assumed, in order to identify the best recipe for our purposes. For this reason, the following considerations were taken into account:

- Firstly, we found that, within the experimental space explored, the X_n variables selected did not significantly affect Y4, Y7, and Y8 responses (see Fig. 6b, Fig. 6c, and Fig. 6d). For this reason, the correspondence of the inks with the behavior of the Ref paste was not considered relevant. In fact, differences in response values between different points are more likely due to random variation than to adjustments controlled by the ink composition.
- Even if the response Y3 was also minimally controlled by the ink composition, bentonite was found to affect the stability of the viscosity in two subsequent printing steps. For this reason, the matching between the value of Y3 with the Ref recipe was not completely excluded, but it was considered less influential than the remaining responses in determining the best recipe.
- The recovery time (Y9 and Y9′) and rest viscosity value (Y5 and Y5′) are considered important parameters for controlling the printing process, however, they are more related to the post-printing step rather than the printing itself. Since the objective of the study has been to replace the Ref recipe with a new one without changing the parameters of the robocasting machine, the accordance in the value of the viscosity at 60 s^{-1} (Y1 and Y1′) with the one of the Ref has been prioritized rather than the other two criteria mentioned above.

The best ink composition has been selected by assigning 1 point to the compositions for which the predicted responses Y1 and Y1′ correspond to the Ref, 0.5 points every time Y5, Y5′, Y9, or Y9′ corresponds, and 0.25 points when Y3. The inks that obtained the highest rank were the numbers 14, 21, and 55 (coded recipes collected in Supplementary S1) which have a predicted value for the viscosity at the nozzle exit (Y1 and Y1′) and resting conditions (Y5) comparable to the one of Ref paste. Among them, the ink number 55 – whose complete composition is given in Table 6 – showed the expected responses comparable to those of the reference. Furthermore, the predicted responses Yn for recipe 55 have been experimentally validated by repeating the measurements through the rotational rheometer on ink with the same composition. All measured parameters were found to be in line with model predictions, except for Y5 and Y5′ which showed a discrepancy. Finally, the ink prepared by using recipe 55 was also printed by means of the robocasting apparatus in the production line of the FZ SoNick SA company. Pictures of the final component after deposition are shown in Fig. S1. The performances obtained by using this new ink were completely comparable to the one shown by the Ref paste; printability and shape fidelity fit all the performance requests by the company without further modification.

4. Conclusions

Accordingly with the aim of the study, the work presented above resulted helpful for a comprehensive characterization of the rheological properties of glass-based ink for robocasting deposition. The promising results obtained by applying DoE and ANOVA on the effect of the components of the ink on its rheological properties highlighted the sognificant effect that solid load has on determining the viscosity of the glass powder suspension at different shear rates. Additionally, the effect of bentonite on determining the rheology of inorganic-based inks was decreased as shear rates increased. However, an opposite trend was observed for the amount of the commercial dispersant Targon.

The knowledge derived from the validated models was also successfully used to tune the ink recipe and adapt its rheological behavior to a standardized printing process in line with industrial-level production. This result showed the possibility of using an original approach which is rheology-based rather than printing process-based with a satisfactory success potential. Such an approach can be beneficial at the industrial level or when, for different reasons, the operator has limited access to modify the printing parameters of a robocasting.

While the intrinsic characteristics of Design of Experiments (DoE) and Analysis of Variance (ANOVA) preclude the generalization of

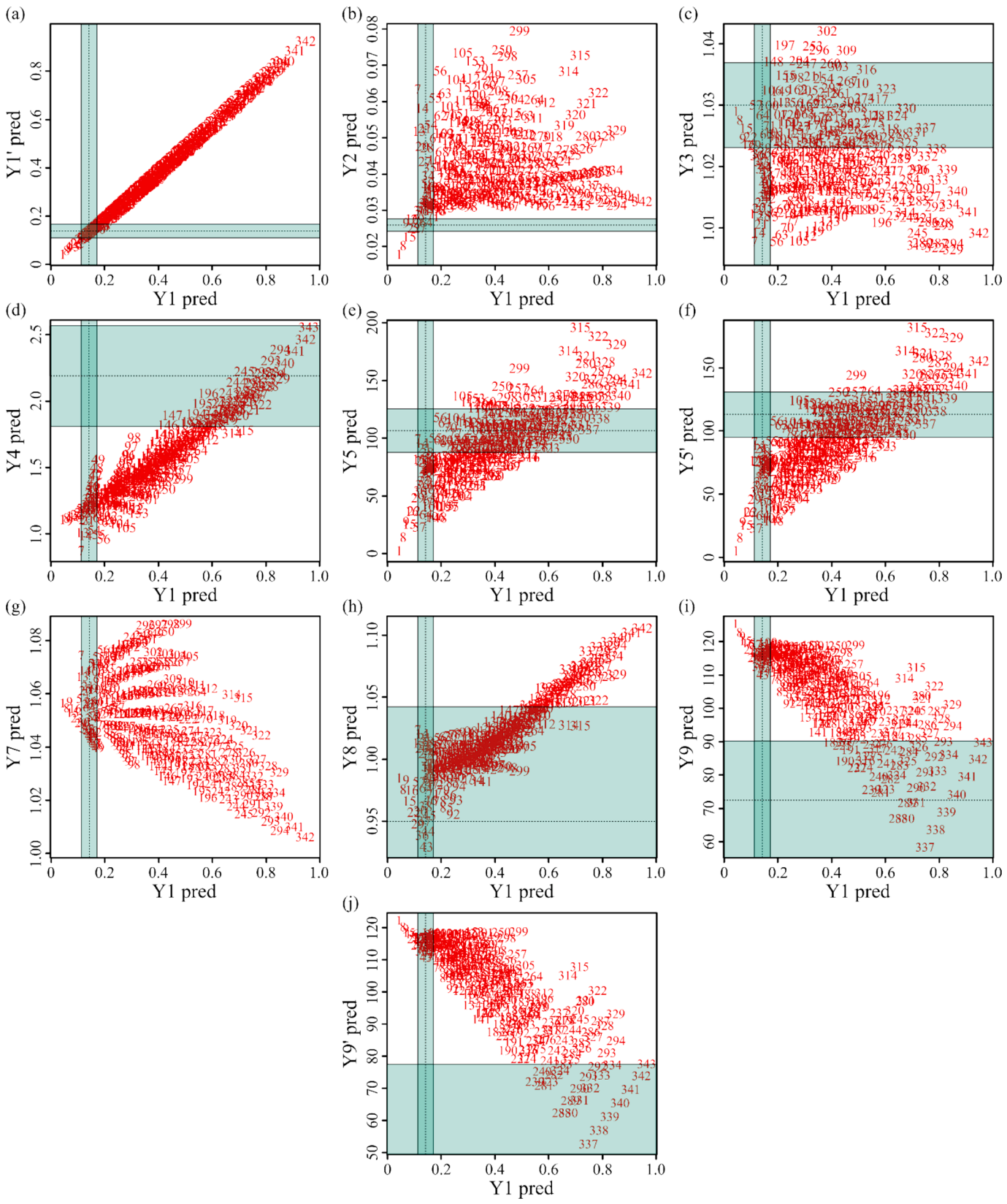

Fig. 7. The values of the responses associated with each point of the test are collected and reported in the graphs above. The interval values representing the target properties are represented by the areas in light blue. When a point (indicated by the number associated) is included inside the area of the target it means that it respects the requirement for that specific response. (For interpretation of the references to colour in this figure legend, the reader is referred to the web version of this article.)

Table 6
Ink recipe that replicates better the rheological behavior of the Ref ink, within the experimental domain primarily selected.

	14 coded values	21 coded values	55 coded values	wt%
water	–	–	–	**38.85 wt%**
Bentonite	**1**	**1**	**0.66**	**1.50 wt%**
fumed silica	**0**	**0**	**0**	**0.12 wt%**
NaCl	**0**	**0**	**0**	**0.03 wt%**
Targon	**−0.66**	**−0.33**	**−1**	**0.00 wt%**
Solid load	**−1**	**−1**	**−0.66**	**59.50 wt%**
G018-402			–	74.0 wt%
Li_2CO_3			–	2.0 wt%
alumina			–	24.0 wt%

conclusions regarding the effects of various compounds on the rheology of the ink beyond the specific experimental domain of this study, this work represents a significant initial effort to develop a systematic approach for optimizing robocasting deposition processes. Specifically, this study underscores the necessity of defining indices that can contribute to standardizing the printability assessment in robocasting.

Although the proposed indices were successfully applied to the case study analyzed here, they may require further refinement to enhance their applicability. For instance, the coefficient of variation defined in this study demonstrated limitations, resulting in a linear model that could not be experimentally validated. While incorporating quadratic coefficients might yield different outcomes, developing a new index to measure the long-term stability of paste viscosity after printing could provide additional insights into process optimization.

This research's findings reaffirm DoE and ANOVA's utility in optimizing and tailoring processes by minimizing the experimental workload, reducing the time required, and lowering associated costs. These methodologies facilitate a more efficient exploration of process variables, underscoring their potential for broader application in advanced manufacturing techniques.

CRediT authorship contribution statement

A. Baggio: Writing – review & editing, Writing – original draft, Visualization, Validation, Methodology, Investigation, Formal analysis, Data curation, Conceptualization. **D. Dalmazzo:** Writing – review & editing, Validation, Supervision, Data curation, Conceptualization. **F. D'Isanto:** Writing – review & editing, Validation, Conceptualization. **E. Santagata:** Writing – review & editing, Resources. **D. Basso:** Writing – review & editing, Resources. **D. Gaia:** Writing – review & editing, Resources. **M. Salvo:** Writing – review & editing, Supervision, Resources, Funding acquisition. **F. Smeacetto:** Writing – review & editing, Supervision, Resources, Funding acquisition.

Declaration of competing interest

The authors declare that they have no known competing financial interests or personal relationships that could have appeared to influence the work reported in this paper.

Acknowledgements

This research was funded by the European Union's Horizon 2020 research and innovation program under grant agreement No 963599 – SOLSTICE, Sodium-Zinc molten salt batteries for low-cost stationary storage.

The authors would like to acknowledge the contribution of Camillo Melzi and Gianmarco Polotti for the R script of the software CAT 4.3 used for the Design of Experiment and ANOVA analysis. Moreover, a sincere thanks to Riccardo Leardi, Emanuele Farnini, and all the research group of Analytical Chemistry and Chemometrics of the Department of Pharmacy, University of Genoa, for the mentorship provided in the frame of the Chemometrics school of Geneva about the DoE.

Appendix A. Supplementary data

Supplementary data to this article can be found online at https://doi.org/10.1016/j.matdes.2025.113678.

Data availability

The data used for the particle size distribution calculations are available at the following DOI: 10.5281/zenodo.13254111 and 10.5281/zenodo.13256429. All the data useful for the replication of the DoE and correlated models are available here: 10.5281/zenodo.13256649.

References

[1] M. Ferraris, S. De la Pierre, Y. Akram, C. Steinborn, G. Puchas, W. Krenkel, High temperature creep behaviour of glass-ceramic joined Nextel 610^{TM}/Al2O3-ZrO2 composites, J. Eur. Ceram. Soc. 42 (2022) 5029–5034, https://doi.org/10.1016/j.jeurceramsoc.2022.04.052.
[2] K.L. Ley, M. Krumpelt, R. Kumar, J.H. Meiser, I. Bloom, Glass-ceramic sealants for solid oxide fuel cells: Part I. Physical properties, J. Mater. Res. 11 (1996) 1489–1493, https://doi.org/10.1557/JMR.1996.0185.
[3] F. Smeacetto, M. Salvo, F.D. D'Hérin Bytner, P. Leone, M. Ferraris, New glass and glass–ceramic sealants for planar solid oxide fuel cells, J. Eur. Ceram. Soc. 30 (2010) 933–940, https://doi.org/10.1016/j.jeurceramsoc.2009.09.033.
[4] I.W. Donald, P.M. Mallinson, B.L. Metcalfe, L.A. Gerrard, J.A. Fernie, Recent developments in the preparation, characterization and applications of glass- and glass–ceramic-to-metal seals and coatings, J Mater Sci 46 (2011) 1975–2000, https://doi.org/10.1007/s10853-010-5095-y.
[5] I.V. Tolstobrov, E.S. Shirokova, A.I. Vepreva, D.Y. Dubovtsev, YuA. Chetvertnykh, A.V. Kuzmin, N.S. Saetova, Fused deposition modeling of glass sealants: A new approach to SOFC sealing, Ceram. Int. 50 (2024) 19561–19570, https://doi.org/10.1016/j.ceramint.2024.03.068.
[6] E. Ercenk, T. Yasar, S. Demirkiran, S. Yilmaz, Glass–ceramic sealant with different alkali contents made from natural and waste materials for SOFC, J Therm Anal Calorim 148 (2023) 4015–4031, https://doi.org/10.1007/s10973-023-12007-5.
[7] A. Drewniak, D. Koszelow, P. Błaszczak, K. Górnicka, K. Jurak, H. Javed, A. G. Sabato, P. Jasiński, S. Molin, F. Smeacetto, Glass-ceramic sealants and steel interconnects: Accelerated interfacial stability and reactivity tests at high temperature, Mater. Des. 212 (2021) 110259, https://doi.org/10.1016/j.matdes.2021.110259.
[8] J.W. Fergus, Sealants for solid oxide fuel cells, J. Power Sources 147 (2005) 46–57, https://doi.org/10.1016/j.jpowsour.2005.05.002.
[9] F. Lantelme, H. Groult. Molten Salts Chemistry : From Lab to Applications, Elsevier, San Diego, United States, 2013, https://doi.org/10.1016/C2012-0-00049-X.
[10] B.L. Ellis, L.F. Nazar, Sodium and sodium-ion energy storage batteries, Curr. Opin. Solid State Mater. Sci. 16 (2012) 168–177, https://doi.org/10.1016/j.cossms.2012.04.002.
[11] M.M. Gross, S.J. Percival, R.Y. Lee, A.S. Peretti, E.D. Spoerke, L.J. Small, A high-voltage, low-temperature molten sodium battery enabled by metal halide catholyte chemistry, Cell Rep. Phys. Sci. 2 (2021) 100489, https://doi.org/10.1016/j.xcrp.2021.100489.
[12] T. Evans, J. Olson, V. Bhat, S.-H. Lee, Corrosion of stainless steel battery components by bis(fluorosulfonyl)imide based ionic liquid electrolytes, J. Power Sources 269 (2014) 616–620, https://doi.org/10.1016/j.jpowsour.2014.07.047.
[13] J. Lee, S.H. Shin, J.K. Lee, S. Choi, J.H. Kim, Corrosion behavior of surface treated steel in liquid sodium negative electrode of liquid metal battery, J. Power Sources 307 (2016) 526–537, https://doi.org/10.1016/j.jpowsour.2016.01.019.
[14] Z. Wen, Y. Hu, X. Wu, J. Han, Z. Gu, Main Challenges for High Performance NAS Battery: Materials and Interfaces, Adv. Funct. Mater. 23 (2013) 1005–1018, https://doi.org/10.1002/adfm.201200473.

[15] V. Manthina, G. Song, P. Singh, M.K. Mahapatra, Silica-free sealing glass for sodium-beta alumina battery, Int. J. Appl. Ceram. Technol. 16 (2019) 887–895, https://doi.org/10.1111/ijac.13093.

[16] F. Smeacetto, M. Radaelli, M. Salvo, D. Di Modugno, A.G. Sabato, V. Casalegno, M. Broglia, M. Ferraris, Glass-ceramic joining material for sodium-based battery, Ceram. Int. 43 (2017) 8329–8333, https://doi.org/10.1016/j.ceramint.2017.03.170.

[17] S. Song, Z. Wen, Y. Liu, J. Lin, X. Xu, Q. Zhang, New glass-ceramic sealants for Na/S battery, J Solid State Electrochem 14 (2010) 1735–1740, https://doi.org/10.1007/s10008-010-1028-6.

[18] J.L. Sudworth, Zebra batteries, J. Power Sources 51 (1994) 105–114, https://doi.org/10.1016/0378-7753(94)01967-3.

[19] K.B. Hueso, M. Armand, T. Rojo, High temperature sodium batteries: status, challenges and future trends, Energ. Environ. Sci. 6 (2013) 734–749, https://doi.org/10.1039/C3EE24086J.

[20] G. Zhang, Z. Wen, J. Yang, X. Wu, J. Zhang, Improvement of the sealing performance for sodium anode based battery by interface optimization of alpha-Al2O3/glass sealant, Solid State Ion. 263 (2014) 140–145, https://doi.org/10.1016/j.ssi.2014.05.019.

[21] J.N. Stuecker, J.E. Miller, R.E. Ferrizz, J.E. Mudd, J. Cesarano, Advanced Support Structures for Enhanced Catalytic Activity, Ind. Eng. Chem. Res. 43 (2004) 51–55, https://doi.org/10.1021/ie030291v.

[22] J. Barberi, A. Nommeots-Nomm, E. Fiume, E. Verné, J. Massera, F. Baino, Mechanical characterization of pore-graded bioactive glass scaffolds produced by robocasting, Biomedical Glasses 5 (2019) 140–147, https://doi.org/10.1515/bglass-2019-0012.

[23] E. Guzi de Moraes, I.M. Ferreira, L.B. Teixeira, L.H. Cartapati, M.T. Souza, A. P. Novaes de Oliveira, Additive manufacturing of cellular structures from recycled soda-lime glass printing inks by robocasting, Ceram. Int. 49 (2023) 6554–6562, https://doi.org/10.1016/j.ceramint.2022.10.270.

[24] S. Lamnini, H. Elsayed, Y. Lakhdar, F. Baino, F. Smeacetto, E. Bernardo, Robocasting of advanced ceramics: ink optimization and protocol to predict the printing parameters - A review, Heliyon 8 (2022) e10651, https://doi.org/10.1016/j.heliyon.2022.e10651.

[25] E. Peng, D. Zhang, J. Ding, Ceramic Robocasting: Recent Achievements, Potential, and Future Developments, Adv. Mater. 30 (2018) 1802404, https://doi.org/10.1002/adma.201802404.

[26] S. Lamnini, F. Baino, G. Montalbano, H. Javed, F. Smeacetto, Printability of carboxymethyl cellulose/glass-containing inks for robocasting deposition in reversible solid oxide cell applications, Mater. Lett. 318 (2022) 132239, https://doi.org/10.1016/j.matlet.2022.132239.

[27] S. Anelli, A. Baggio, D. Ferrero, D. Schmider, J. Dailly, M. Santarelli, F. Smeacetto, Characterization and testing of glass-ceramic sealants for protonic ceramic electrolysis cells applications, Ceram. Int. 50 (2024) 17520–17531, https://doi.org/10.1016/j.ceramint.2024.02.240.

[28] S.B. Balani, S.H. Ghaffar, M. Chougan, E. Pei, E. Şahin, Processes and materials used for direct writing technologies: A review, Results Eng. 11 (2021) 100257, https://doi.org/10.1016/j.rineng.2021.100257.

[29] E. Feilden. Additive Manufacturing of Ceramics and Ceramic Composites via Robocasting, Doctor of Philosophy, Imperial College, London, 2017, https://doi.org/10.13140/RG.2.2.29343.25765.

[30] B.A.E. Ben-Arfa, A.S. Neto, I.M. Miranda Salvado, R.C. Pullar, J.M.F. Ferreira, Robocasting, Prediction of ink printability in solgel bioactive glass, Journal of the American Ceramic Society 102 (2019) 1608–1618, https://doi.org/10.1111/jace.16092.

[31] R.A. Fisher, The Design of Experiments, Haffner Press, New York, 1935.

[32] R. Patel, N. Patel, M. Patel, Design, development and optimization of new high performance thin-layer chromatography method for quantitation of Retapamulin in pharmaceutical formulation: Application of design of experiment, Sep. Sci. Plus 3 (2020) 121–128, https://doi.org/10.1002/sscp.201900107.

[33] H.H. Ly, S. Daniel, S.K.V. Soriano, Z. Kis, A.K. Blakney, Optimization of Lipid Nanoparticles for saRNA Expression and Cellular Activation Using a Design-of-Experiment Approach, Mol. Pharmaceutics 19 (2022) 1892–1905, https://doi.org/10.1021/acs.molpharmaceut.2c00032.

[34] R. Rebollo, F. Oyoun, Y. Corvis, M.M. El-Hammadi, B. Saubamea, K. Andrieux, N. Mignet, K. Alhareth, Microfluidic Manufacturing of Liposomes: Development and Optimization by Design of Experiment and Machine Learning, ACS Appl. Mater. Interfaces 14 (2022) 39736–39745, https://doi.org/10.1021/acsami.2c06627.

[35] J. Antony, Improving the wire bonding process quality using statistically designed experiments, Microelectron. J. 30 (1999) 161–168, https://doi.org/10.1016/S0026-2692(98)00104-9.

[36] H. Rowlands, J. Antony, Application of design of experiments to a spot welding process, Assem. Autom. 23 (2003) 273–279, https://doi.org/10.1108/01445150310486549.

[37] B.C.Y. Lee, M.S. Mahtab, T.H. Neo, I.H. Farooqi, A. Khursheed, A comprehensive review of Design of experiment (DOE) for water and wastewater treatment application - Key concepts, methodology and contextualized application, J. Water Process Eng. 47 (2022) 102673, https://doi.org/10.1016/j.jwpe.2022.102673.

[38] C. Alex Mbachu, A. Kamoru Babayemi, T. Chinedu Egbosiuba, J. Ifeanyichukwu Ike, I. Jacinta Ani, S. Mustapha, Green synthesis of iron oxide nanoparticles by Taguchi design of experiment method for effective adsorption of methylene blue and methyl orange from textile wastewater, Results Eng. 19 (2023) 101198, https://doi.org/10.1016/j.rineng.2023.101198.

[39] H.K. Mamidi, S. Palekar, P.K. Nukala, S.M. Mishra, M. Patki, Y. Fu, P. Supner, G. Chauhan, K. Patel, Process optimization of twin-screw melt granulation of fenofibrate using design of experiment (DoE), Int. J. Pharm. 593 (2021) 120101, https://doi.org/10.1016/j.ijpharm.2020.120101.

[40] I. Flores Ituarte, O. Wiikinkoski, A. Jansson, Additive Manufacturing of Polypropylene: A Screening Design of Experiment Using Laser-Based Powder Bed Fusion, Polymers 10 (2018) 1293, https://doi.org/10.3390/polym10121293.

[41] K.M. Sharif, M.M. Rahman, J. Azmir, A. Mohamed, M.H.A. Jahurul, F. Sahena, I.S. M. Zaidul, Experimental design of supercritical fluid extraction – A review, J. Food Eng. 124 (2014) 105–116, https://doi.org/10.1016/j.jfoodeng.2013.10.003.

[42] S.-H. Lee, J. Park, H.-R. Kim, T. Lee, J. Lee, Y.-O. Im, C.-H. Lee, H. Cho, H. Lee, C.-H. Jun, Y.-C. Ahn, I.-B. Lee, K.-H. Lee, Synthesis of carbon nanotube fibers using the direct spinning process based on Design of Experiment (DOE), Carbon 100 (2016) 647–655, https://doi.org/10.1016/j.carbon.2016.01.034.

[43] R. Leardi, Chapter 2 - Experimental Design, in: F. Marini (Ed.), Data Handling in Science and Technology, Elsevier, 2013: pp. 9–53. https://doi.org/10.1016/B978-0-444-59528-7.00002-8.

[44] B. Benedetti, V. Caponigro, F. Ardini, Experimental Design Step by Step: A Practical Guide for Beginners, Crit. Rev. Anal. Chem. 52 (2022) 1015–1028, https://doi.org/10.1080/10408347.2020.1848517.

[45] J. Antony, 4 - A Systematic Methodology for Design of Experiments, in: J. Antony (Ed.), Design of Experiments for Engineers and Scientists (second Edition), Second Edition, Elsevier, Oxford, 2014, pp. 33–50, https://doi.org/10.1016/B978-0-08-099417-8.00004-3.

[46] M. Ji, H.-J. Shim, J.H. Kim, Y.-S. Lee, J.P. Choi, Y.-I. Lee, Processing parameter correlations in powder bed fusion additive manufacturing for Fe–Si soft magnetic materials through design of experiments, Powder Metall. (2023) 1–11, https://doi.org/10.1080/00325899.2023.2239599.

[47] D. Gourdonnaud, V. Pateloup, A. Junger, J. Bourret, T. Chartier, P.-M. Geffroy, Correlation between filament deposition path, microstructural and mechanical properties of dense alumina parts printed by robocasting, J. Eur. Ceram. Soc. 44 (2024) 1027–1035, https://doi.org/10.1016/j.jeurceramsoc.2023.09.067.

[48] A. Renteria, H. Fontes, J.A. Diaz, J.E. Regis, L.A. Chavez, T.-L. (Bill) Tseng, Y. Liu, Y. Lin, Optimization of 3D printing parameters for BaTiO3 piezoelectric ceramics through design of experiments, Mater. Res. Express 6 (2019) 085706, https://doi.org/10.1088/2053-1591/ab200e.

[49] I. Buj-Corral, A. Domínguez-Fernández, A. Gómez-Gejo, Effect of Printing Parameters on Dimensional Error and Surface Roughness Obtained in Direct Ink Writing (DIW) Processes, Materials 13 (2020) 2157, https://doi.org/10.3390/ma13092157.

[50] S. Przybyła, M. Kwiatkowski, M. Kwiatkowski, M. Hebda, Optimization of Ceramic Paste Composition for 3D Printing via Robocasting, Materials 17 (2024) 4560, https://doi.org/10.3390/ma17184560.

[51] M. Maillard, J. Chevalier, L. Gremillard, G.P. Baeza, E.-J. Courtial, S. Marion, V. Garnier, Optimization of mechanical properties of robocast alumina parts through control of the paste rheology, J. Eur. Ceram. Soc. 43 (2023) 2805–2817, https://doi.org/10.1016/j.jeurceramsoc.2022.12.008.

[52] S. Tang, L. Yang, X. Liu, G. Li, W. Jiang, Z. Fan, Direct ink writing additive manufacturing of porous alumina-based ceramic cores modified with nanosized MgO, J. Eur. Ceram. Soc. 40 (2020) 5758–5766, https://doi.org/10.1016/j.jeurceramsoc.2020.07.058.

[53] M.-C. Li, Q. Wu, K. Song, C.F. De Hoop, S. Lee, Y. Qing, Y. Wu, Cellulose Nanocrystals and Polyanionic Cellulose as Additives in Bentonite Water-Based Drilling Fluids: Rheological Modeling and Filtration Mechanisms, Ind. Eng. Chem. Res. 55 (2016) 133–143, https://doi.org/10.1021/acs.iecr.5b03510.

[54] D.M. Marum, M.D. Afonso, B.B. Ochoa, Rheological behavior of a bentonite mud, Appl. Rheol. 30 (2020) 107–118, https://doi.org/10.1515/arh-2020-0108.

[55] H.-M. Cho, W. Yoo, B. Yoo, Effect of NaCl Addition on Rheological Behaviors of Commercial Gum-Based Food Thickener Used for Dysphagia Diets, Prev Nutr Food Sci 20 (2015) 137–142, https://doi.org/10.3746/pnf.2015.20.2.137.

[56] A. Amiri, G. Øye, J. Sjöblom, Influence of pH, high salinity and particle concentration on stability and rheological properties of aqueous suspensions of fumed silica, Colloids Surf A Physicochem Eng Asp 349 (2009) 43–54, https://doi.org/10.1016/j.colsurfa.2009.07.050.

[57] J.-H. So, S.-M. Yang, C. Kim, J.C. Hyun, Microstructure and rheological behaviour of electrosterically stabilized silica particle suspensions, Colloids Surf A Physicochem Eng Asp 190 (2001) 89–98, https://doi.org/10.1016/S0927-7757(01)00668-9.

[58] M. Kawaguchi, Dispersion stability and rheological properties of silica suspensions in aqueous solutions, Adv. Colloid Interface Sci. 284 (2020) 102248, https://doi.org/10.1016/j.cis.2020.102248.

[59] G. Franchin, L. Wahl, P. Colombo, Direct ink writing of ceramic matrix composite structures, J. Am. Ceram. Soc. 100 (2017) 4397–4401, https://doi.org/10.1111/jace.15045.

[60] F. D'Isanto, A. Baggio, M. Salvo, D. Basso, D. Gaia, F. Smeacetto, Glass-based sealants for joining α to β''-Al2O3 in Na–Zn batteries, Ceram. Int. 50 (2024) 14542–14549, https://doi.org/10.1016/j.ceramint.2024.01.367.

[61] L.M. Rodríguez-Lorenzo, J.M.F. Ferreira, Development of porous ceramic bodies for applications in tissue engineering and drug delivery systems, Mater. Res. Bull. 39 (2004) 83–91, https://doi.org/10.1016/j.materresbull.2003.09.014.

[62] J.M.F. Ferreira, H.M.M. Diz, Effect of Solids Loading on Slip-Casting Performance of Silicon Carbide Slurries, J. Am. Ceram. Soc. 82 (1999) 1993–2000, https://doi.org/10.1111/j.1151-2916.1999.tb02031.x.

[63] P. Goos, B. Jones. Optimal Design of Experiments: A Case Study Approach, John Wiley & Sons, Incorporated, Newark, UNITED KINGDOM, 2011, https://doi.org/10.1002/9781119974017.

[64] M. Zhou, Z. Wu, X. Ouyang, X. Hu, C. Shi, Mixture design methods for ultra-high-performance concrete - a review, Cem. Concr. Compos. 124 (2021) 104242, https://doi.org/10.1016/j.cemconcomp.2021.104242.
[65] M.A. Bezerra, V.A. Lemos, C.G. Novaes, R.M. de Jesus, H.R.S. Filho, S.A. Araújo, J. P.S. Alves, Application of mixture design in analytical chemistry, Microchem. J. 152 (2020) 104336, https://doi.org/10.1016/j.microc.2019.104336.
[66] R.F. Gunst, R.L. Mason, Fractional factorial design, WIREs Comput. Stat. 1 (2009) 234–244, https://doi.org/10.1002/wics.27.
[67] A. M'Barki, L. Bocquet, A. Stevenson, Linking Rheology and Printability for Dense and Strong Ceramics by Direct Ink Writing, Sci Rep 7 (2017) 6017, https://doi.org/10.1038/s41598-017-06115-0.
[68] B.A.E. Ben-Arfa, A.S. Neto, I.E. Palamá, I.M. Miranda Salvado, R.C. Pullar, J.M. F. Ferreira, Robocasting of ceramic glass scaffolds: Sol–gel glass, new horizons, J. Eur. Ceram. Soc. 39 (2019) 1625–1634, https://doi.org/10.1016/j.jeurceramsoc.2018.11.019.
[69] Y. Lin, H. Qin, J. Guo, J. Chen, Rheology of bentonite dispersions: Role of ionic strength and solid content, Appl. Clay Sci. 214 (2021) 106275, https://doi.org/10.1016/j.clay.2021.106275.